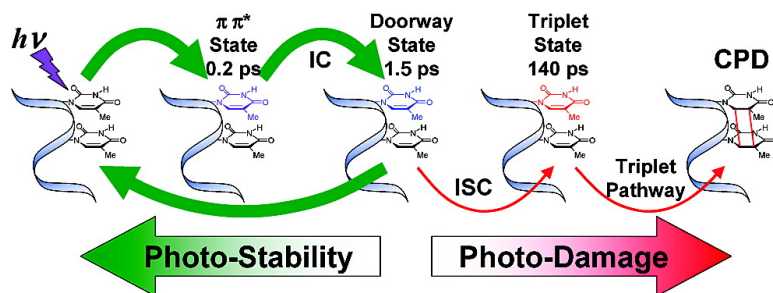# A Doorway State Leads to Photostability
or Triplet Photodamage in Thymine DNA

Wai-Ming Kwok, Chensheng Ma, and David Lee Phillips

More About This Article

Additional resources and features associated with this article are available within the HTML version:

- Supporting Information
- Links to the 2 articles that cite this article, as of the time of this article download
- Access to high resolution figures
- Links to articles and content related to this article
- Copyright permission to reproduce figures and/or text from this article

View the Full Text HTML

A Doorway State Leads to Photostability or Triplet Photodamage in Thymine DNA

Wai-Ming Kwok,*,† Chensheng Ma,*,‡ and David Lee Phillips*,‡

Department of Applied Biology and Chemical Technology, The Hong Kong Polytechnic University, Hung Hom, Kowloon, Hong Kong, China, and Department of Chemistry, The University of Hong Kong, Pokfulam Road, Hong Kong, China

Received October 12, 2007; E-mail: bcwmkwok@polyu.edu.hk; macs@hkucc.hku.hk; phillips@hkucc.hku.hk

Abstract: Ultraviolet irradiation of DNA produces electronic excited states that predominantly eliminate the excitation energy by returning to the ground state (photostability) or following minor pathways into mutagenic photoproducts (photodamage). The cyclobutane pyrimidine dimer (CPD) formed from photodimerization of thymines in DNA is the most common form of photodamage. The underlying molecular processes governing photostability and photodamage of thymine-constituted DNA remain unclear. Here, a combined femtosecond broadband time-resolved fluorescence and transient absorption spectroscopies were employed to study a monomer thymidine and a single-stranded thymine oligonucleotide. We show that the protecting deactivation of a thymine multimer is due to an ultrafast single-base localized stepwise mechanism where the initial excited state decays via a doorway state to the ground state or proceeds via the doorway state to a triplet state identified as a major precursor for CPD photodamage. These results provide new mechanistic characterization of and a dynamic link between the photoexcitation of DNA and DNA photostability and photodamage.

Introduction

DNA is the major cellular target of UV irradiation, and sequences containing two or multiple pyrimidine bases are mutational hotspots that have been linked with a range of human health problems.[1,2] Intrastrand pyrimidine dimerization is the most common photochemical process initiated by UV excitation of DNA. The dimerization leads the two adjacent pyrimidines within the same DNA strand to become covalently linked, and this, for the case of TT sequences, yields mostly the four-membered ring cyclobutane pyrimidine dimer (CPD) dimers, a small amount of pyrimidine 6-4 pyrimidone photoproduct (6-4PP), and related Dewar-valence isomers (Dews).[3,4] The TT CPD, dominated by the *cis—syn* CPD form, is among the most abundant photolesions in UV-excited native DNA.[1,3,4] Since the

first isolation of the TT dimers more than four decades ago,[5,6] there has been intense research interest in understanding how and to what extent the initial singlet excited state (S_{FC}) populated directly by photoabsorption of 200–300 nm UV light can evolve and transform into these photoproducts. This has motivated extensive photophysical and photochemical studies on various relevant aspects for a wide range of systems including thymine monomers,[7–13] thymine-constituted oligomers,[9,14–16] and DNAs.[3,4,13,15,16] For thymine monomers, the S_{FC} population predominantly deactivates nonradiatively on a subpicosecond time scale to recover the ground state (S_0)[7,8] or to produce a minor yield of a triplet excited state (T_1).[9,10] Photosensitization

---

† The Hong Kong Polytechnic University.
‡ The University of Hong Kong.
(1) Cadet, J.; Vigny, P. In *The Photochemistry of Nucleic Acids*; Morrison, H., Ed.; Wiley: New York, 1990; pp 1–272.
(2) (a) Borgdorff, V.; Pauw, B.; Hees-Stuivenberg, S.; Wind, N. *DNA Repair* **2006**, *5*, 1364–1372. (b) Ikehata, H.; Ono, T.; Tanaka, K.; Todo, T. *DNA Repair* **2007**, *6*, 658–668. (c) Nijhof, J. G. W.; Mulder, A. M.; Speksnijder, E. N.; Hoogervorst, E. M.; Mullenders, L. H. F.; Gruijl, F. R. *DNA Repair* **2007**, *6*, 1642–1650. (d) Queille, S.; Luron, L.; Spatz, A.; Avril, M. F.; Ribrag, V.; Duvillard, P.; Hiesse, C.; Sarasin, A.; Armand, J. P.; Daya-Grosjean, L. *Carcinogenesis* **2007**, *28*, 724–731.
(3) (a) Douki, T.; Court, M.; Sauvaigo, S.; Odin, F.; Cadet, J. *J. Biol. Chem.* **2000**, *275*, 11678–11685. (b) Douki, T.; Angelov, D.; Cadet, J. *J. Am. Chem. Soc.* **2001**, *123*, 11360–11366. (c) Douki, T.; Reynaud-Angelin, A.; Cadet, J.; Sage, E. *Biochemistry* **2003**, *42*, 9221–9226. (d) Douki, T. *J. Photochem. Photobiol. B: Biol.* **2006**, *83*, 45–52. (e) Cadet, J.; Courdavault, S.; Ravanat, J. L.; Douki, T. *Pure Appl. Chem.* **2005**, *77*, 947–961.
(4) Becker, M. M.; Wang, Z. *J. Mol. Biol.* **1989**, *210*, 429–438.

(5) (a) Beukers, R.; Berends, W. *Biochim. Biophys. Acta* **1960**, *41*, 550–551. (b) Beukers, R.; Ijlstra, J.; Berends, W. *Rec. Trav. Chim.* **1960**, *79*, 101–104.
(6) (a) Wulff, D. L.; Fraenkel, G. *Biochim. Biophys. Acta* **1961**, *51*, 332–339. (b) Johns, H. E.; Pearson, M. L.; LeBlanc, J. C.; Helleiner, C. W. *J. Mol. Biol.* **1964**, *9*, 503–524.
(7) (a) Pecourt, J. L.; Peon, J.; Kohler, B. *J. Am. Chem. Soc.* **2001**, *123*, 10370–10378. (b) Pecourt, J. L.; Peon, J.; Kohler, B. *J. Am. Chem. Soc.* **2000**, *122*, 9348–9349.
(8) Crespo-Hernández, C. E.; Cohen, B.; Hare, P. M.; Kohler, B. *Chem. Rev.* **2004**, *104*, 1977–2019.
(9) Marguet, S.; Markovitsi, D. *J. Am. Chem. Soc.* **2005**, *127*, 5780–5781.
(10) Salet, C.; Bensasson, R.; Becker, R. S. *Photochem. Photobiol.* **1979**, *30*, 325–329.
(11) Lamola, A. A.; Yamane, T. *Proc. Natl. Acad. Sci. U.S.A.* **1967**, *58*, 443–446.
(12) Lamola, A. A.; Mittal, J. P. *Science* **1966**, *154*, 1560–1561.
(13) Moysan, A.; Viari, A.; Vigny, P.; Voituriez, L.; Cadet, J.; Moustacchi, E.; Sage, E. *Biochemistry* **1991**, *30*, 7080–7088.
(14) Schreier, W. J.; Schrader, T. E.; Koller, F. O.; Gilch, P.; Crespo-Hernández, C. E.; Swaminathan, V. N.; Carell, T.; Zinth, W.; Kohler, B. *Science* **2007**, *315*, 625–629.
(15) Nikogosyan, D. N. *Int. J. Radiat. Biol.* **1990**, *57*, 233–299.
(16) (a) Görner, H. *J. Photochem. Photobiol. B: Biol.* **1994**, *26*, 117–139. (b) Görner, H. *Photochem. Photobiol.* **1990**, *52*, 935–948.

experiments and the dependence of the CPD formation efficiency on triplet quenchers (such as oxygen) has established the T_1 state as the reactive precursor with the CPD formation described as a diffusion-controlled bimolecular reaction with one thymine in T_1 and the other in S_0.[1,11-13] However, it remains unknown whether this scenario applies to CPD generation in DNA or thymine oligomers, where the thymine units are organized and held closely together.

The uncertainty about the CPD formation mechanism in the assembled systems arises mainly from the complexity of the interaction between the nearby thymine chromophores that may substantially modify the nature and depopulation dynamics of the excited states[17-24] to cause the physical conversion and chemical reaction channels for DNA or thymine oligomers to be substantially different from those observed for the thymine monomers. A specific issue subject to long-standing controversy regards the singlet vs triplet nature of the excited state as an origin of the TT CPD formation in DNA.[9,15,16] On the one hand, triplet photosensitization experiments confirm the presence of a triplet-mediated CPD formation mechanism.[1,3a,11,13,15,16] On the other hand, from consideration of the structural flexibility and the close proximity of neighboring bases in oligomers or DNAs as well as the observation of the lack of an appreciable oxygen quenching effect, singlet mechanisms either bypassing or competing with the triplet pathway have been proposed for the CPD generation.[14-16] A recent time-resolved infrared (TRIR) study presented evidence for an ultrafast formation of $cis-syn$ CPD ($\sim$1 ps) in a thymine oligomer $(dT)_{18}$ and supports the singlet mechanism.[14] Gas-phase theoretical modeling on systems containing two structurally stacked thymines reports possible singlet pathways responsible for the rapid CPD generation.[25] Computational investigations considering solvent effects suggest the probability of the triplet pathway to account for the CPD photoproduct.[26] To justify the role played by the triplet-mediated CPD photochemistry in UV-excited DNA damage requires unambiguous assessment on whether an "intrinsic" UV-absorption induced triplet pathway exists or the triplet pathway turns out to be accessible only with the presence of an added "external" photosensitizer so as to populate the DNA triplet through a triplet-to-triplet energy transfer mechanism. We note that despite the pivotal importance of the reactive triplet state, the generation dynamics and UV-excitation promoted intersystem crossing (ISC) to yield such a state has not been

characterized and observed directly in previous studies for either thymine monomers or DNAs and oligomers containing thymine. Moreover, details of the elementary excited-state events underlying the S_{FC} deactivation pathways and their relevance to photostability and photodamage have remained elusive for both the monomeric and multimeric thymines. There are also great uncertainties on how the conformational arrangement and interaction in the assembled systems may influence the S_{FC} depopulation and how this may consequently affect the precise electronic character, the dynamics, and the reactivity of the involved excited states.

To help address these issues, we report here a broadband ultrafast time-resolved fluorescence (TRF) and transient absorption (TA) spectroscopic study providing simultaneous real-time monitoring and comparative spectral characterization of the excited-state processes for a free thymidine (dT) monomer and a single-stranded thymine oligonucleotide, $(dT)_{20}$. The $(dT)_{20}$ oligomer has a dimerization quantum yield of $\sim$0.028 (among the highest reported for DNAs).[9] Comparing it with the monomeric dT affords an ideal model system to explore the CPD generation mechanism in thymine oligomer. Complementary information provided by the broadband TRF and TA measurements combined with the high sensitivity and broad spectral and time detection window of our femtosecond techniques allows us to unravel the dynamics and fundamental events involved in temporal evolution of the S_{FC} through various electronic states and to evaluate their connection with the nonreactive, protecting conversion channels or the reactive, damaging transformation channels associated with the CPD formation. Comparison of the data obtained for dT and $(dT)_{20}$ reveals a significant similarity in many aspects between the two systems and shows the presence of a doorway state that leads to either the ground state (photostability) or a triplet-mediated CPD generation pathway for UV-irradiated thymine oligomers.

Experimental Method

The experimental set-ups and spectral calibrations are described elsewhere.[18,27,28] The TRF and TA measurements were performed based on a commercial Ti:sapphire regenerative amplifier laser system. The samples were excited by a 267 nm pump pulse, and subsequent photoinduced excited states were probed by a second pulse using TRF and TA techniques. In the TRF measurements, a Kerr-gate technique[29,30] was employed. A 1 mm thick fused silica plate Kerr medium equipped with a crossed polarizer pair was driven by a 800 nm probe pulse to act as an ultrafast shutter to sample the fluorescence spectra at various pump/probe delay times. In the TA experiments, the sample was probed by a white light continuum pulse. The time window for both kinds of measurements extends from femtoseconds to $\sim$2 ns. The spectral window for the TRF and TA measurements covers the $\sim$270-700 nm and 300-700 nm regions, respectively. The IRF of the ultrafast system is wavelength-dependent and varies from $\sim$250 to $\sim$350 fs for TRF and $\sim$150 to $\sim$250 fs for TA as the wavelength varies from 600 to 280 nm. To avoid unwanted multiphoton or saturation effects, the power of the pump laser pulse was kept as low as possible with a typical laser pulse peak power $\sim$2 GW/cm^2 being used. The dT and $(dT)_{20}$ were purchased from Sigma-Aldrich (with >99% purity)

(17) Eisinger, J.; Shulman, R. G. *Science* **1968**, *161*, 1311–1319.

(18) Kwok, W.-M.; Ma, C.; Phillips, D. L. *J. Am. Chem. Soc.* **2006**, *128*, 11894–11905.

(19) Crespo-Hernández, C. E.; Cohen, B.; Kohler, B. *Nature* **2005**, *436*, 1141–1144.

(20) (a) Markovitsi, D.; Talbot, F.; Gustavsson, T.; Onidas, D.; Lazzarotto, E.; Marguet, S. *Nature* **2006**, *441* (7094), E7–E7. (b) Markovitsi, D.; Onidas, D.; Gustavsson, T.; Talbot, F.; Lazzarotto, E. *J. Am. Chem. Soc.* **2005**, *127*, 17130–17131. (c) Markovitsi, D.; Gustavsson, T.; Talbot, F. *Photochem. Photobiol. Sci.* **2007**, *7*, 717–724.

(21) Plessow, R.; Brockhinke, A.; Eimer, W.; Kohse-Höinghaus, K. *J. Phys. Chem. B* **2000**, *104*, 3695–3704.

(22) (a) Buchvarov, I.; Wang, Q.; Raytchev, M.; Trifonov, A.; Fiebig, T. *Proc. Natl. Acad. Sci. U.S.A.* **2007**, *104*, 4794–4797. (b) Wang, Q.; Raytchev, M.; Fiebig, T. *Photochem. Photobiol.* **2007**, *83*, 637–641.

(23) Santoro, F.; Barone, V.; Improta, R. *Proc. Natl. Acad. Sci. U.S.A.* **2007**, *104*, 9931–9936.

(24) Crespo-Hernández, C. E.; Kohler, B. *J. Phys. Chem. B* **2004**, *108*, 11182–11188.

(25) (a) Boggio-Pasqua, M.; Groenhof, G.; Schäfer, L. V.; Grubmüller, H.; Robb, M. A. *J. Am. Chem. Soc.* **2007**, *129*, 10996–10997. (b) Blancafort, L.; Migani, A. *J. Am. Chem. Soc.* **2007**, *129*, 14540–14541.

(26) (a) Zhang, R. B.; Eriksson, L. A. *J. Phys. Chem. B* **2006**, *110*, 7556–7562. (b) Durbeej, B.; Eriksson, L. A. *J. Photochem. Photobiol., A* **2002**, *151*, 95–101.

(27) Ma, C.; Kwok, W. M.; Chan, W. S.; Zuo, P.; Kan, J. T. W.; Toy, P. H.; Phillips, D. L. *J. Am. Chem. Soc.* **2005**, *127*, 1463–1427.

(28) Ma, C.; Kwok, W. M.; Chan, W. S.; Du, Y.; Kan, J. T. W.; Toy, P. H.; Phillips, D. L. *J. Am. Chem. Soc.* **2006**, *128*, 2558–2570.

(29) Matousek, P.; Towrie, M.; Ma, C.; Kwok, W-M.; Phillips, D.; Toner, W. T.; Parker, A. W. *J. Raman Spectrosc.* **2001**, *32*, 983–988.

(30) Matousek, P.; Towrie, M.; Stanley, A.; Parker, A. W. *Appl. Spectrosc.* **1999**, *53*, 1485–1489.
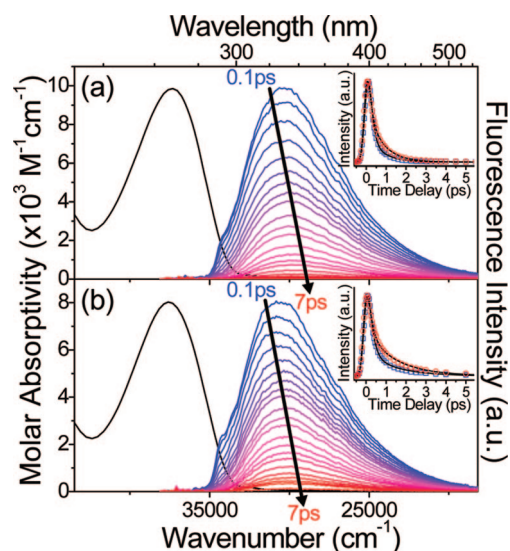
Figure 1. Temporal evolution of the broadband TRF spectra of 267 nm excited (a) dT and (b) $(dT)_{20}$ obtained in a buffered aqueous solution (pH = 6.8) with an identical absorbance at the excitation wavelength. The UV-absorption spectra (solid black lines) of dT and $(dT)_{20}$ are also displayed in panels (a) and (b), respectively. The insets show normalized time dependence of the fluorescence decay dynamics of (a) dT and (b) $(dT)_{20}$ at 300 nm (□) and 335 nm (○) wavelengths obtained from the corresponding TRF spectra. The solid lines in the insets represent the instrumental response function (IRF) convoluted two-exponential fitting of the experimental data. For each system, the simulations were done with the same set of two time constants but weighted by different proportionality factors.
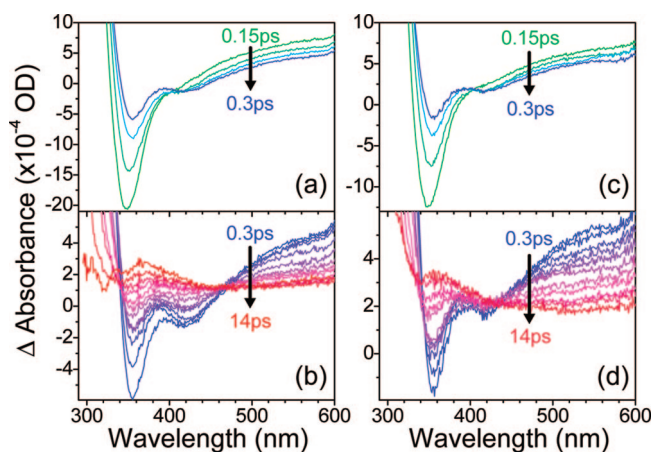
and Sigma Proligo with RPC purification (~90% purity), respectively. Solutions of tridistilled water were used for the experiments. The samples were flowed in a cell with CaF_2 windows for the measurements. Samples were monitored for photodegradation by UV absorption spectroscopy during the measurements and replaced with fresh ones as needed.

Results and Discussion

1. Ultrafast Broadband Time-Resolved Spectra. The dynamics of the fluorescent ("bright") singlet excited state(s) involved in the S_{FC} relaxation processes were examined by acquisition of the TRF spectra for dT and $(dT)_{20}$. Analogous TA experiments were done (i) to explore whether a "dark" singlet nature state also participates in the S_{FC} relaxation and (ii) to look for the ISC pathway leading to the generation of the triplet state.

Comparison of the TRF results obtained with 267 nm excitation is displayed in Figure 1a,b for dT and $(dT)_{20}$, respectively. The 267 nm excitation of dT populates a strongly allowed $^1\pi\pi^*$ state (denoted hereafter by S_π) of the thymine chromophore.[31–34] The $(dT)_{20}$ UV-absorption spectrum (Figure 1b) and the initial transient fluorescence spectrum (the 0.1 ps TRF spectrum in Figure 1b) strongly resemble those of the corresponding dT spectra (see Supporting Information, part A, for details of the spectral comparison). Hence, we can attribute the S_{FC} state of $(dT)_{20}$ to a state of similar intrinsic electronic character ($^1\pi\pi^*$), with its excitation localized on one thymine unit.

Figure 2. Transient absorption spectra of (a, b) dT and (c, d) $(dT)_{20}$ at early times before 0.3 ps and early picosecond times (0.3−14 ps) recorded in buffered aqueous solution with an identical absorbance at the 267 nm excitation wavelength.

The observed ultrafast decay (see insets in Figure 1) and TRF evolution for dT and $(dT)_{20}$ are due to the S_π depopulation relaxation of the predominant canonical diketo form of the thymine moiety.[7,8,32,35] The minor enol−keto thymine tautomer (with ~2% population) and products of the probable S_π proton-exchange or phototautomerization reaction exhibit relatively long-lived and deeply red-shifted fluorescence with λ_{max} at ~390−405 nm.[35–38] The absence of these types of fluorescence components in the TRF spectra indicates no significant contribution from these species. Fitting the wavelength-dependent decay curves (especially at the blue region) required summing two exponential functions convoluted with the TRF instrument response function (IRF). Global analysis at various wavelengths resulted in time constants of ~0.15 ps (τ_1) and ~0.76 ps (τ_2) for dT and ~0.20 ps (τ_1) and ~1.50 ps (τ_2) for $(dT)_{20}$ that are generally consistent with recent single-wavelength (330 nm) fluorescence up-conversion studies on these or closely related systems.[33,39–41]

The initial broadband transient absorption (TA) temporal evolution of the dT and $(dT)_{20}$ spectra in Figure 2a,c show a decrease of the ~400–600 nm signal and a simultaneously increase of the 310–400 nm absorption combined with two isosbestic points at ~410 and ~310 nm (see also Supporting Information, Figure 1S). This clearly indicates a direct dynamical conversion from one state into a second state. The second state spectra continues to evolve (Figure 2b,d) and weak absorption bands with λ_{max} at ~365 nm grow in at the expense of the 440–600 nm and <340 nm absorptions with isosbestic points at ~440 and ~340 nm. This demonstrates transformation from the second state to a third state. From their close resemblance to the well-characterized T_1 spectra of the thymidine mono-

(31) Lorenton, J.; Fülscher, M. P.; Roos, B. O. *J. Am. Chem. Soc.* **1995**, *117*, 9265–9273.

(32) Broo, A.; Holmén, A. *J. Phys. Chem. A* **1997**, *101*, 3589–3600.

(33) Gustavsson, G.; Bányász, Á.; Lazzarotto, E.; Markovitsi, D.; Scalmani, G.; Frisch, M. J.; Barone, V.; Improta, R. *J. Am. Chem. Soc.* **2006**, *128*, 607–619.

(34) Perun, S.; Sobolewski, A. L.; Domcke, W. *J. Phys. Chem. A* **2006**, *110*, 13238–13244.

(35) Morsy, M. A.; Al-Somali, A. M.; Suwaiyan, A. *J. Phys. Chem. B* **1999**, *103*, 11205–11210.

(36) Suwaiyan, A.; Morsy, M. A.; Odah, K. A. *Chem. Phys. Lett.* **1995**, *237*, 349–355.

(37) Markova, N.; Enchev, V.; Timtcheva, I. *J. Phys. Chem. A* **2005**, *109*, 1981–1988.

(38) Hanus, M.; Kabeláč, M.; Nachtigallová, A.; Hobza, P. *Biochemistry* **2005**, *44*, 1701–1707.

(39) (a) Onidas, D.; Markovitsi, D.; Marguet, S.; Sharonov, A.; Gustavsson, T. *J. Phys. Chem. B* **2002**, *106*, 11367–11374. (b) Gustavsson, T.; Sharonov, A.; Markovitsi, D. *Chem. Phys. Lett.* **2002**, *351*, 195–200.

(40) Markovitsi, D.; Sharonov, A.; Onidas, D.; Gustavsson, T. *ChemPhysChem* **2003**, *3*, 303–305.

(41) Peon, J.; Zewail, A. H. *Chem. Phys. Lett.* **2001**, *348*, 255–262.

phosphate (TMP),[9,10] and the fact that the T_1 absorption spectrum exhibits negligible qualitative variation upon going from the thymine base to the nucleoside to the nucleotide,[42] the latter spectra with λ_{max} at 365 nm can be attributed confidently to the T_1 of the thymine chromophore for both dT and $(dT)_{20}$.

The temporal evolution of the TA spectra for dT and $(dT)_{20}$ can be described by a kinetic model of

$$1 \xrightarrow{\tau_1} 2 \xrightarrow{\tau_2} T \xrightarrow{\tau_3} P \qquad (1)$$

where τ_1 and τ_2 represent conversion time constants for the $1 \rightarrow 2$ (<0.3 ps) and the $2 \rightarrow T$ (<10 ps) transformations, respectively, and τ_3 corresponds to the decay time constant of the T_1 state to P (denoted generally as the "product" from the T_1 decay). The subnanosecond spectra showing decay of T_1 in $(dT)_{20}$ is given in the Supporting Information, Figure 2S. Correlated global analysis based on a three-exponential function convolved with the IRF satisfactorily fitted the TA intensity profile at various wavelengths >320 nm to yield time constants of 0.15 ps (τ_1), 0.76 ps (τ_2), and 4000 ps (τ_3) for dT and 0.2 ps (τ_1), 1.50 ps (τ_2), and 140 ps (τ_3) for $(dT)_{20}$. Typical experimental and fitting results of the TA dynamics for dT and $(dT)_{20}$ at representative wavelengths of ~300, ~350, ~370, ~470, and ~570 nm are displayed in Figure 3. The TA decay at ~570 nm is biexponential and is due to the combined decay dynamics from states 1 and 2. The ~370 nm TA temporal profile shows the exclusive dynamical characterization for the formation and subsequent decay of the T_1 state. The ISC transformation of state 2 into T_1 is shown clearly from the good match in the dynamics of the picosecond growth at 370 nm and the corresponding decay at 570 nm (Figure 3). The temporal TA profile in the wavelength region below 320 nm (Figure 3c,f) does not follow the three-exponential kinetics due to the additional contributions from vibrational cooling (VC) dynamics of the hot S_0 that is repopulated by the prompt IC decay[7,8] (see Supporting Information, part B, for details).

2. Deactivation via a Doorway State. Comparison of the TA visible region dynamics and the TRF data clearly shows that the excited-state τ_1/τ_2 times from the TA results for dT and $(dT)_{20}$ coincide very well with the corresponding TRF τ_1/τ_2 time constants. This indicates that both measurements are probing the same excited-state processes for states 1 and 2. Thus, state 1 detected by the TA measurements is assigned to the S_π state probed by the TRF measurements. State 2 observed in the TA and TRF results is attributed to a second singlet excited state (denoted as S_x) that has not been identified before. Thus, the TRF spectra (Figure 1) recorded at the early (0.1 ps) and late (>4 ps) times can be taken as representative spectra due to the S_π and S_x states, respectively, for the two compounds.(see Supporting Information, Figure 3S, and part C for details of these spectra).

Intrinsic S_π and S_x fluorescence spectra for dT and $(dT)_{20}$ were obtained by wavelength-dependent analysis (see Supporting Information, Figure 5S, and part D). The spectral parameters derived from log-normal simulation of these spectra are listed in Table 1. With an estimate of radiation rate constant (k^f) for S_π (k_1^f) and the k_1^f/k_2^f ratio and assuming a unit conversion efficiency from S_π to S_x, the k_2^f of S_x was calculated to be ~0.6 $\times 10^8$ and ~0.4 $\times 10^8$ s^{-1} for dT and $(dT)_{20}$, respectively (see

(42) Gut, I. G.; Wood, P. D.; Redmond, R. W. *J. Am. Chem. Soc.* **1996**, *118*, 2366–2373.
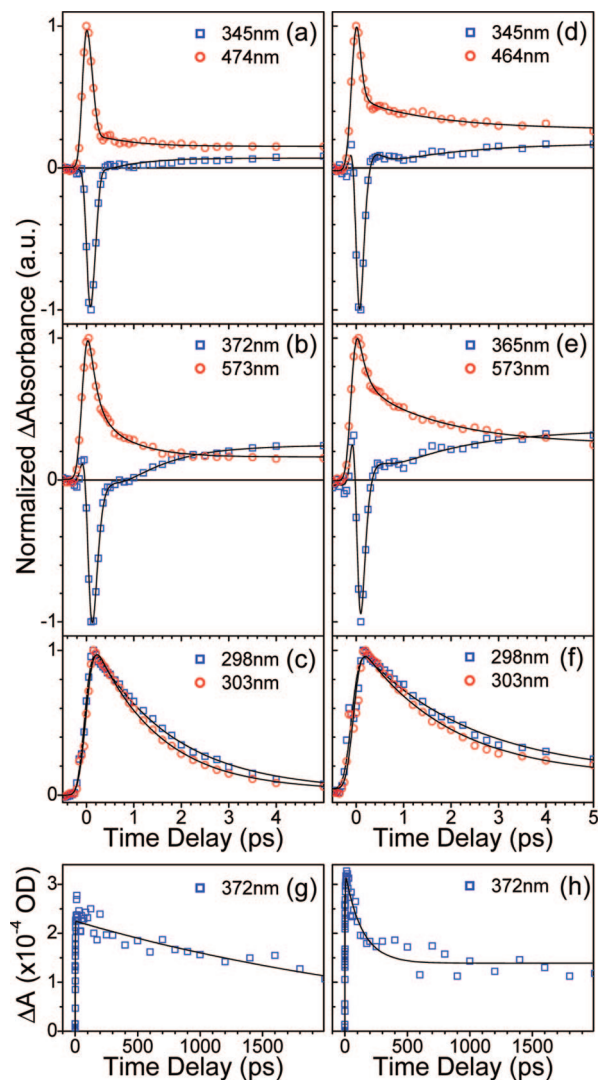
Figure 3. Time dependence of the transient absorbance for (a–c) dT and (d–f) $(dT)_{20}$ at various wavelengths as labeled in the figure obtained from the TA spectra in Figure 2. The triplet state decay dynamics are displayed in panels g and h for dT and $(dT)_{20}$, respectively, as determined from the time dependence of the triplet absorption at ~372 nm (λ_{max}). The solid lines represent kinetic fittings of the experimental profiles based on simulations employing three-exponential functions convolved with the IRF.

Supporting Information part E, for details). This allows one to estimate a total fluorescence quantum yield (given as $\varphi_f = k_1^f\tau_1 + k_2^f\tau_2$) of ~0.8 $\times 10^{-4}$ for dT and 1.0 $\times 10^{-4}$ for $(dT)_{20}$ (Table 1). The calculated yield for dT agrees well with literature experimental values ((0.9–1.3) $\times 10^{-4}$) for the same compound[1,39,43] and provides further support for the involvement of the two singlet states within the IC deactivation pathway. Since a hypothesis of a fractional S_π to S_x conversion efficiency leads to an estimated φ_f substantially different from literature experimental values, the assumption of a near unit conversion appears reasonable. Therefore, a near-unity $S_\pi \rightarrow S_x$ transformation is proposed as the first step to depopulate S_π. This and the TA observation of the S_0 recovery and ensuing VC indicates that a consecutive depopulation scheme of $S_\pi \rightarrow S_x \rightarrow S_0$ (hot) $\rightarrow S_0$ can be constructed for the IC decay pathway to account for the photostability of dT against UV excitation. By analogy,

(43) Callis, P. R. *Annu. Rev. Phys. Chem.* **1983**, *34*, 329–357.

Table 1. Spectral Parameters of the Excited-State Lifetimes (τ), the Fluorescence Peak Positions (λ^{fluo}), the Maximum Extinction Coefficients (ϵ_{max}), the Radiative Rate Constants (k^{fluo}), the Fluorescence Quantum Yields (φ_{fluo}) and the Intersystem Crossing Yields (φ_{ISC}) Obtained from TRF and TA Spectral Analysis of dT and (dT)$_{20}$ in Aqueous Solution

	dT	(dT)$_{20}$
τ_1 (ps)	0.15	0.20
τ_2 (ps)	0.76	1.50
τ_3 (ps)	4000	140
λ_1^{fluo} (nm)	329	326
λ_2^{fluo} (nm)	338	335
ϵ_{max} ($\times 10^3$ M^{-1} cm^{-1})	9.8^a	8.0
k_1^{fluo} ($\times 10^8$ s^{-1})	2.2	1.8
k_2^{fluo} ($\times 10^8$ s^{-1})	0.6	0.4
φ_{fluo}^{calcd} ($\times 10^{-4}$)	0.8	1.0
φ_{fluo}^{exptl} ($\times 10^{-4}$)	0.9 (1.0, 1.3)^{a,b}	
φ_{ISC} ($\times 10^{-2}$)	1.4^c	2.8–3.0

^{a} From ref 39a. ^{b} From ref 43. ^{c} From refs 9 and 10.

the same IC decay channel for (dT)$_{20}$ is also proposed. The photostability of the (dT)$_{20}$ oligomer originates from the intrinsic photostability of the constituent thymine base units and is barely influenced by the tethered sugar–phosphate backbone. This is consistent with the single-wavelength TA study by Kohler and co-workers who found a generally similar IC pathway for TMP and (dT)$_{18}$.[14,19]

The IC pathway suggested here for dT is different from pathways reported in earlier studies.[33,44] The major difference is the involvement of the modestly "bright" S$_x$ state within the IC processes. This state may have been detected in previous relevant single-wavelength femtosecond studies,[7,19,33,39–41,44a] but the lack of wavelength resolution together with the similar lifetimes, as well as strong spectral overlap with spectra of the S$_\pi$ state (both fluorescence and absorption), probably contributed to the inability to differentiate this state clearly from the S$_\pi$ state. Our results for the IC pathway, in conjunction with the kinetic scheme (1) revealed by the TA data, indicate unequivocally that the newly identified S$_x$ is the key intermediate or doorway state that governs the partitioning of the excited-state population between the two photophysical relaxation channels for the prevailing IC from the S$_\pi$ to S$_0$ and the small ISC conversion that yields the T$_1$ state for both dT and (dT)$_{20}$.

3. Decay of the T$_1$ State and CPD Formation. The T$_1$ state of dT is an electronic $^3\pi\pi^*$ state[10,42,45] with an experimental yield (φ_T) reported to be $\sim 1.4 \times 10^{-2}$ in aqueous solution.[10,11] The direct observation here of the ISC and triplet absorption spectrum under identical photoabsorption conditions for dT and (dT)$_{20}$ allows a comparison of the corresponding TA spectra between the two compounds and can be used to estimate the so far unknown important parameter of the triplet yield for (dT)$_{20}$. The resemblance of the ISC dynamics and the T$_1$ absorption profile (represented by the 14 ps TA spectra in Figure 2) for (dT)$_{20}$ and those of dT convincingly suggest an analogous electronic nature of a thymine-localized T$_1$ for (dT)$_{20}$ as for the $^3\pi\pi^*$ of dT. Neglecting the hypochromic effect in (dT)$_{20}$, the T$_1 \rightarrow$ T$_n$ extinction coefficient (ϵ_T) of the T$_1$ TA spectra should be about the same for both systems. From this, a φ_T of $\sim 2.1 \times 10^{-2}$ for (dT)$_{20}$ can be deduced based on the published dT φ_T value[10,11] and the ratio of the recorded absorbance at ~ 370 nm (λ_{max}) of the fully developed dT vs (dT)$_{20}$ T$_1$ spectra and the

differences of the triplet decay dynamics for both systems (Figure 3g,h). A corrected φ_T value of $(2.8–3) \times 10^{-2}$ can be estimated for (dT)$_{20}$ when hypochromism is present by assuming a ~ 25–30% drop in ϵ_T for (dT)$_{20}$ compared with dT.[46] Notwithstanding the uncertainty in the precise value of φ_T for (dT)$_{20}$, it is clear that φ_T is modestly larger for (dT)$_{20}$ than dT. This is consistent with the increase in φ_T upon going from the TMP monomer to an aggregated thymine and a TpT deoxydinucleotide postulated in early ESR studies.[47]

Comparison of the T$_1$ decay dynamics between dT and (dT)$_{20}$ (Figure 3 g,h) provides a connection between the T$_1$ state and CPD formation in an oligomer system. For dT in aqueous solution at room temperature, the possible deactivation processes that could contribute to the ~ 4 ns depletion of the T$_1$ population include[9–12,42,48] (i) bimolecular diffusion-controlled self-quenching by addition of a dT in T$_1$ to a S$_0$ dT molecule leading to either CPD production or S$_0$ dT recovery, (ii) bimolecular quenching of dT T$_1$ by oxygen in the sample, and (iii) spontaneous unimolecular decay of dT T$_1$ to S$_0$. Considering a typical oxygen concentration of $\sim 10^{-3}$–10^{-4} M, a diffusion-limited oxygen quenching rate constant[10,15,16,42,48] of $\sim 4 \times 10^9$ M^{-1} s^{-1}, and a natural T$_1$ lifetime of several to tens of microseconds for dT,[9,10,15,16,48] processes ii and iii are too slow to account for the observed T$_1$ decay dynamics. Therefore, process (i) should be the major cause for the T$_1$ decay dynamics. The $\sim(4$–$5) \times 10^{-3}$ M experimental concentration gives a $\sim 10^{10}$ M^{-1} s^{-1} self-quenching rate constant (k_{sq}), consistent with the high efficiency of the T$_1$ self-quenching for thymine monomers as reported in the literature.[15,16,42,48] Over the 10^{-4} to 10^{-5} M range, the literature k_{sq}[15,16,48] ranges from 3×10^9 to 1×10^8 M^{-1} s^{-1}. The estimated k_{sq} here is close to the highest reported values due to the higher sample concentration used in our TA measurements and probably reflects a strong tendency of the T$_1$ dT to combine with a nearby accessible S$_0$ molecule under high-concentration conditions. Within this context and considering the general common nature of the T$_1$ for (dT)$_{20}$ and that of dT, the much faster T$_1$ decay observed in (dT)$_{20}$ than dT can be explained by the close proximity of the neighboring thymine units constrained by the sugar–phosphate backbone in (dT)$_{20}$, making the self-quenching an intramolecular type of event, which greatly facilitates the quenching dynamics.

From the above analysis and combined with (i) the almost oligomer conformation insensitive IC and ISC dynamics and the general similarity in the electronic nature of the involved excited states (S$_\pi$, S$_x$, and T$_1$) for dT and (dT)$_{20}$, (ii) the faster T$_1$ quenching dynamics for (dT)$_{20}$ (~ 140 ps time constant) than dT (~ 4 ns time constant), and (iii) the reactivity of T$_1$ toward CPD production for both dT and (dT)$_{20}$ as established by previous photosensitization studies,[1,11–13] it is compelling to suggest that the T$_1$ state is a major precursor to the photodimerization reaction for (dT)$_{20}$. The estimated φ_T for (dT)$_{20}$ here is close to the ~ 0.028 CPD yield reported for this system.[9] This may suggest an almost complete crossover of the T$_1$ population into CPD products if the T$_1$ reaction is the only pathway leading to CPD formation. A remarkably high T$_1$ to CPD transformation efficiency was reported for sensitized thymine photodimerization in DNA.[11,17] Additionally, our observed ~ 140 ps triplet decay

(44) (a) Hare, P. M.; Crespo-Hernández, C. E.; Kohler, B. *Proc. Natl. Acad. Sci. U.S.A.* **2007**, *104*, 435–440. (b) Hare, P. M.; Crespo-Hernández, C. E.; Kohler, B. *J. Phys. Chem. B* **2006**, *110*, 18641–18650.

(45) Shulman, R. G.; Rahn, R. O. *J. Chem. Phys.* **1966**, *45*, 2940–2946.

(46) (a) Tinoco, I. *J. Am. Chem. Soc.* **1960**, *83*, 4765–4789. (b) Rhoders, W. *J. Am. Chem. Soc.* **1961**, *83*, 3609–3617.

(47) Lamola, A. A.; Guéron, M.; Yamane, T.; Eisinger, J.; Shulman, R. G. *J. Chem. Phys.* **1967**, *47*, 2210–2217.

(48) Whillans, D. W.; Johns, H. E. *J. Am. Chem. Soc.* **1971**, *93*, 1358–1362.

Scheme 1. Schematic Energy Diagram Showing the Proposed Major Deactivation and Reaction Pathways for 267 nm Photoexcited (a) dT and (b) $(dT)_{20}$ in Aqueous Solution[a]
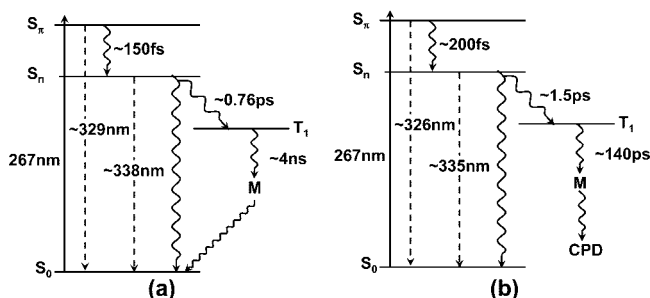
[a] The dashed lines with the wavelength values indicate the fluorescence deactivation of the corresponding states; the curved lines indicate nonradiative deactivation pathways with corresponding decay time constants labeled for the related excited states. The "M" refers to the biradical intermediate involved in the T_1 self-quenching reaction (see text for details).

dynamics in $(dT)_{20}$ provides an explanation for the apparent lack of an oxygen quenching effect reported in previous studies for CPD formation in assembled DNA systems.[16] The diffusion-controlled oxygen quenching process is simply too slow to compete with the intramolecular triplet quenching reaction that subsequently leads to the CPD product. The "P" in eq 1 is thus attributed to the CPD for $(dT)_{20}$. UV absorption of $(dT)_{20}$ recorded before and after the time-resolved experiments (Supporting Information, Figure 5S) confirms the generation of a substantial amount of CPD upon 267 nm excitation.

In contrast, parallel UV–vis measurements for dT reveal only a minor change in the UV absorption implying that the monomer T_1 quenching, though efficient, gives only a very low yield of CPD. This is consistent with the common observation of inefficient T_1 self-quenching to produce CPDs for various dilute thymine monomer systems.[42,48,49] Experimental and theoretical studies suggest that this inefficiency is due to a transient biradical species in the T_1 self-quenching reaction that subsequently reverts mainly into two S_0 molecules with only a small fraction collapsing into CPD.[26a,49,50] Thus, the "P" in eq 1 for dT is attributed to the S_0 molecule as the major "photoproduct" and CPD as the minor "byproduct". A modest offset-like signal was observed in the T_1 decay (Figure 3g,h and Supporting Information, Figure 2S) at late picosecond times and persists up to early nanosecond times for both dT and $(dT)_{20}$, and this is also consistent with a radical intermediate for a stepwise T_1 dimerization. In this case, a nanosecond time scale dynamics for the CPD formation is expected. To summarize the preceding discussion and analyses of the TRF and TA results, a deactivation scheme describing the IC conversion to the S_0 and the T_1-mediated CPD formation pathway for 267 nm excited dT and $(dT)_{20}$ is presented in Scheme 1.

As mentioned in the Introduction, besides the major CPD product, UV excitation of the bipyrimidine TT sites inducing dimerization also leads to a minor amount of the 6-4PP photoproduct. The TT 6-4PP product is believed to form via a competitive Paterno–Buchi photocycloaddition reaction and is mediated by a transient oxetane precursor that may involve a singlet excited state.[1,9,15,16,25b] Bearing in mind the rather low yield (about 1 order of magnitude less than the CPD formation) of the 6-4PP compared with CPD,[1,9,15,16] our present results on

dT and $(dT)_{20}$ do not allow explicit discussion on the specific excited-state channel associated with the 6-4PP formation. However, the absence of the characteristic 6-4PP absorption band (with λ_{max} at ∼325 nm) in the recorded TA spectra (Figure 2 and Figure 2S) at time delays from femtoseconds up to several nanoseconds suggests a much slower formation dynamics for the 6-4PP adduct. This appears consistent with a recent nanosecond laser flash photolysis study showing that the 6-4PP product of 267 nm excited $(dT)_{20}$ is formed within the microsecond time scale.[9]

Our preceding elucidation of the dT and $(dT)_{20}$ S_{FC} deactivation in terms of the branching between the major protective IC conversion and the minor intrinsic triplet CPD photochemical channel demonstrates the importance of the combined application of broadband TRF and TA spectroscopy in deciphering and identifying the elementary steps and the relevant excited states involved in the UV-excited processes of a DNA monomer and oligomer. TRF spectroscopy is a powerful approach to detect the dynamics of the relevant fluorescent singlet excited state(s). The TA spectroscopy can provide information not only on the fluorescent state(s) but also on dark states including weakly fluorescent or "dark" singlet excited states, the triplet excited states, and other transient species like radicals, ions, etc. Combining the complementary TA data that may have information on the dark states with a comparison/correlation of the TA and TRF dynamics on the common fluorescent singlet excited states provides a powerful method to evaluate explicitly the electronic character of the observed transient states and to reveal comprehensively the associated photophysical and photochemical conversions. Indeed, previous ultrafast studies report significant involvement of "dark" and weakly fluorescent excited states with lifetimes ranging from several picoseconds to several nanoseconds in the S_{FC} depopulation for some DNA or RNA bases and various oligomer systems.[8,18–21,24,40,44] Depending on the identity of the free nucleobases or sequences of the DNA oligomers, these states have been associated with the lowest S_n singlet state (for example, pyrimidine bases in aqueous solution),[44a] the excitation-energy delocalized excimer singlet excited state (as found for oligomers composed of consecutive adenine and cytosine),[18,19,21,24] and the triplet excited state.[44b] In this regard, the combined TRF and TA results here present the first effort to our knowledge to provide direct experimental femtosecond broadband spectral evidence for an unequivocal assessment of the electronic nature and dynamics of the excited states integrated in the S_{FC} evolution for UV-excited monomeric thymine base and thymine oligomer. We are now extending our work to other systems especially oligomers with mutational hotspots of dicytosine or cytosine containing bipyrimidine sites.[1,2]

The degree of photostability and propensity toward photodamage for a DNA oligomer system is determined by the relative accessibility of the S_{FC} population to nonreactive excited states vs a reactive triplet state. The known nonreactive states include generally the S_π ("bright") and possibly the S_n (which are modestly fluorescent, see section D below) singlet states involved in the return-to-S_0 IC pathway of the free bases.[8,18,19,33,44] For single-stranded oligomers and DNA assemblies, in addition to this, by preventing localization of the excitation energy on a single base residue, rapid and efficient formation of an excimer state may supply an alternative process to prevent the system from accessing the triplet reaction pathway.[18] For double-stranded DNA, prompt light-initiated interstrand proton or hydrogen transfer between paired bases can also serve as a

(49) Wagner, P. J.; Bucheck, D. J. *J. Am. Chem. Soc.* **1970**, *92*, 181–185.
(50) Wagner, P. J.; Bucheck, D. J. *J. Am. Chem. Soc.* **1969**, *91*, 5090–5097.

protective pathway to compete with the ISC channel.[51] The excimer state is characterized by a long-lived (hundreds of picoseconds lifetime) weak fluorescence band that appears at a significantly red-shifted spectral region with respect to the corresponding monomer fluorescence spectrum.[8,17,18,21] The absence of such a feature in our single-stranded $(dT)_{20}$ TRF spectra (see Figure 1b and Figure 3S) and in the combined TA and TRF dynamics analyses suggests that there is little contribution of the excimer state to the $(dT)_{20}$ S_{FC} deactivation. Given the importance of the interbase stacking interaction in mediating the excimer state formation,[18,19,24] the apparent absence of such a state for $(dT)_{20}$ may well be associated with the inherent high flexibility, random orientation, and weakly stacking character of the thymine oligomer and polymer.[52] This together with the relatively high triplet yield of thymine (among the highest within the four DNA bases)[15,16] might suggest that thymine runs in DNA are inherently weak segments toward UV irradiation and they may act as traps for the photoexcitation energy. This could possibly account for the well-established fact that the two and multiple thymine bases in DNA sequences are the most efficient photoreactive sites resulting in CPD formation.[1,3,4,15,16] This implies further that the dynamic picture of the triplet-mediated CPD pathway (Scheme 1b) is applicable to the CPD photodamage in natural DNA. In this regard, the observation of the dicytosine site in DNA being far less photoreactive[1–3] may be due to the availability of the excimer state for consecutive cytosine-containing single-stranded oligomer[17,21] or the availability of the proton or hydrogen transfer pathway between the G—C pair for the related double-stranded systems.[51a] Other factors such as the dynamics and the sequences and conformations of the secondary structure could also contribute to the sequence-dependent variation of DNA photostability.[1,3,4,15,16]

Differing from our T_1 predominant CPD formation pathway, the TRIR study[14] reported that thymine CPD formation is an ultrafast process finished within ~1 ps after UV excitation and proposed a singlet (S_π) dimerization pathway. Although the results here give no evidence for substantial involvement of the singlet excited state(s) in the photodimerization reaction, one cannot preclude the singlet mechanism since the fairly low CPD yield makes it difficult to explicitly identify the precise origin of formation. It is possible that the triplet and singlet pathways may both contribute with different weighting factors to the dimerization reaction. Additional rigorous experimental evidence on direct CPD-forming dynamics over a broad temporal window covering the femtosecond to nanosecond time scales is needed to provide a definitive assessment of this issue.

4. Nature of the Doorway State. A noteworthy point that deserves discussion is the assignment of the newly identified S_x state in view of its important role in the overall deactivation processes (see Scheme 1), especially in the bifurcation of the initial S_{FC} (S_π) population between the IC to the S_0 pathway and the ISC to the T_1 state. According to the fluorescence data obtained for the S_x and S_π states and the conversion dynamics of S_x in connection with the S_0, S_π, and T_1 states (see Table 1), the S_x state ought to possess the following features: (i) it can

afford a rather effective ISC to the T_1, since based on the data of φ_f, φ_T, and k_f, an ISC rate of on the order of 10^{10} s^{-1} in magnitude can be derived suggesting an allowed nature for the ISC transition;[53] (ii) in accordance with the acquired S_x fluorescence profile and its large overlap with the S_π profile, the energy of the S_x state is expected to be close to but slightly lower than that of the S_π state; (iii) the S_x state can be easily accessible from the S_π state and subsequently to the S_0 state so as to be consistent with our observed ultrafast IC dynamics; (iv) the S_x state is a modestly "bright" state as manifested by its radiative rate, which is on the 10^7 s^{-1} order of magnitude.[53] With these criteria and taking into account the results of previous studies especially those of sophisticated theoretical investigations based on *ab initio* computations,[31,33,34,54–56] we can make some constructive remarks on the possible attribution of the S_x state.

Thymine, like all the other DNA and RNA bases, possesses a series of closely spaced and low-lying excited states classified by electronic transition of $\pi\pi^*$ and $n\pi^*$ character.[8,31–34,44,54–60] Among these states, the lowest-energy $\pi\pi^*$ and $n\pi^*$ states and their interplay are decisively important in the nonradiative decay of the bases, especially the pyrimidine bases.[8,33,34,54–59] For thymine, the lowest $\pi\pi^*$ state carries significant oscillator strength corresponding to the optically prepared S_π state;[31–34] the lowest $n\pi^*$ state has its n → π^* transition associated with the C_4=O_8 carbonyl group[32–34,55] corresponding to the earlier mentioned S_n and this state appears to be the most likely candidate that could meet the criteria described in the previous paragraph. First, considering the $\pi\pi^*$ nature of the T_1 state and being in accordance with the classical propensity rule (the El-Sayed rule),[53] the allowed nature of the S_x → T_1 ISC (the criterion i) suggests and requires the S_x to be a state with substantial $n\pi^*$ character to mediate the correlated spin–orbital coupling (SOC). Second, high-level energy calculations on thymine in the gas phase have shown that the S_n state is lower in energy than the nearby S_π state at both the S_0 equilibrium geometry and their respective energy-minimized geometries.[31,34] Computations including solvent effects suggest that the S_n state could remain as the lowest emitting excited state even in aqueous solution.[55] On the basis of Kasha's rule, this knowledge of the energetic state ordering supports and agrees with the S_n ascription to the observed lower energy and relatively longer-lived fluorescence spectrum (criterion ii). Third, the accessibility of the S_n state from the S_π state and to the S_0 state (criterion iii) has been subject to extensive theoretical studies;[31–34,54–57] despite the fact that there still are some discrepancies as to details of the potential surface topology, most of the recent calculations suggest consistently that there are extensive coupling region(s) (conical intersection (CI)) present involving all three states and specific out-of-plane vibrational modes (such

(51) (a) Sobolewski, A. L.; Domcke, W.; Hattig, C. *Proc. Natl. Acad. Sci. U.S.A.* **2005**, *102*, 17903–17906. (b) Schultz, T.; Samoylova, E.; Radloff, W.; Hertel, I. V.; Sobolewski, A. L.; Domcke, W. *Science* **2004**, *306*, 1765–1768. (c) Schwalb, N. K.; Temps, F. *J. Am. Chem. Soc.* **2007**, *129*, 9272–9273.

(52) (a) Camerman, N.; Fawcett, J. K.; Camerman, A. *J. Mol. Biol.* **1976**, *107*, 601–621. (b) Martinez, J. M.; Elmroth, S. K. C.; Kloo, L. *J. Am. Chem. Soc.* **2001**, *123*, 12279–12289. (c) Mills, J. B.; Vacano, E.; Hagerman, P. L. *J. Mol. Biol.* **1999**, *285*, 245–257.

(53) Turro, N. J. *Modern Molecular Photochemistry*; University Science Book: Mill Valley, CA, 1991.

(54) (a) Merchán, M.; Serrano-Andrés, L.; Robb, M. A.; Blancafirt, L. *J. Am. Chem. Soc.* **2005**, *127*, 1820–1825. (b) Blancafirt, L.; Robb, M. A. *J. Phys. Chem. A* **2004**, *108*, 10609–10614.

(55) Improta, R.; Barone, V. *J. Am. Chem. Soc.* **2004**, *126*, 14320–14321.

(56) (a) Matsika, S. *J. Phys. Chem. A* **2004**, *108*, 7584–7590. (b) Matsika, S. *J. Phys. Chem. A* **2005**, *109*, 7538–7545.

(57) (a) Marian, C. M.; Schneider, F.; Kleinschmidt, M.; Tatchen, J. *Eur. Phys. J.* **2002**, *D20*, 357–367. (b) Marian, C. M. *J. Chem. Phys.* **2005**, *122*, 104314.

(58) Ismail, N.; Blancafirt, L.; Olivucci, M.; Kohler, B.; Robb, M. A. *J. Am. Chem. Soc.* **2002**, *124*, 6818–6819.

(59) Merchán, M.; Serrano-Andrés, L. *J. Am. Chem. Soc.* **2003**, *125*, 8108–8109.

(60) Cohen, B.; Crespo-Hernández, C. E.; Kohler, B. *Faraday Discuss.* **2004**, *127*, 137–147.

as twisting of a pyrimidine C=C bond and pyramidalization of the relevant carbonyl group) needed to reach the CIs have been identified.[33,54,56] It is essential to mention that vibronic coupling (VC) between the nearby S_π and S_n states promoted by the out-of-plane modes has been frequently invoked as a mechanism (the "proximity effect") for the rapid nonradiative $S_1 \rightarrow S_0$ conversion exhibited by the nucleobases.[8,54,56,57a,61–63] Finally, we note that the modest "bright" feature of the S_x state (criterion iv) seems to be somewhat inconsistent with the presumed "dark" nature of the S_n attributed state. This complexity, provides, however, new insight into the electronic features of the S_n in regard that it can be readily accommodated by the perception of some S_π/S_n vibronic coupling that may result in a S_n state of mixed nature that borrows some oscillator strength from the S_π state.[64,65] In fact, theoretical studies on cytosine[54] have reported the existence of such a mixed character state from the S_π/S_n vibronic interaction along the pyrimidalization coordinate and more importantly the work[54a] also finds that its presence can induce high SOC that favors the ISC to yield the $\pi\pi^*$ T_1 state. This provides further support for the role of mediating ISC that we attribute to the S_x state.

Based on the above considerations, we provisionally assign the S_x state to a S_n state of mixed nature and denote it as S_n' for clearness (Scheme 1). We consider the S_n' state as the long sought after but not yet confirmed so-called "dark" state discussed numerous times in the literature. It appears that this assignment combined with the well-known solvent effect of water could afford a consistent and common interpretation to the reported thymine IC dynamics in both the solution phase and the gas phase. This also sheds some light on many intriguing solvent-dependent spectroscopic observations reported in the literature for thymine and its derivatives.

With the S_n' assignment, we come to a two-step IC deactivation path of $S_\pi \rightarrow S_n' \rightarrow S_0$ for dT and (dT)$_{20}$. The underlying mechanistic picture of this decay pathway is as follows: after excitation into the S_π state, vibronic coupling that is facilitated by the relevant out-of-plane vibration(s) promptly drives (with a time constant of τ_1, see Table 1) the excited-state population into the S_n' state. This is followed by a fast (with a time constant of τ_2, see Table 1) nonradiative decay of S_n' to S_0 by IC to produce a vibrationally hot S_0, the key step of transferring the electronic energy into heat. The hot S_0 is subsequently cooled by heat transfer to the surrounding solvent. Given the very rapid nature of the S_n' to S_0 decay; it is highly plausible that the conversion proceeds through a low-barrier CI due to a surface crossing of these two states. We note that, although this mechanism differs from those proposed in previous studies of thymine in aqueous solution,[33,44a] it is virtually identical to the decay pathway suggested by most gas-phase studies[66–68] and some theoretical calculations[34,54–57] except that these studies

consider the S_n state, rather than the S_n' state, as the intermediate "relay" state.

Comparison of the deactivation dynamics reported for thymine in the gas phase[66–69] and in aqueous solution[33,39,44a] shows that time constants of the first step (τ_1) are quite similar (~0.1–0.2 ps) in both cases while the second step time constant (τ_2) is substantially longer in the gas phase (~6 ps as reported in refs 66–68 and tens of nanoseconds in refs 69a and 69b) than in aqueous solution (~0.7 ps).[33,39] Considering the similarity of τ_1 in both environments, it is rational that the S_π/S_n VC would be the common mechanism to depopulate the initially photoprepared S_π under either environmental condition. It is interesting that this ultrafast state switch brought about by the out-of-plane conformational change(s) may account for the broad and diffusive feature of the fluorescence spectrum reported for thymine in the gas phase,[70] and it could also contribute to the fairly large Stokes shift displayed by the fluorescence/absorption spectra (Figure 1). The S_π mixed character of the S_n' state may explain the modestly lower value of the fluorescence anisotropy observed for thymine in aqueous solution.[39]

On the other hand, the difference in the τ_2 time constants between the gas phase and aqueous solution can be reconciled by taking into account the solvent effect that introduces a perturbation to the potential energy landscape. In aqueous solution, the solvent polarity and especially the solute–solvent hydrogen-bonding interaction can cause an energy increase of the S_n state relative to the S_π state.[33,54–57,71–74] For thymine and most of its derivatives, this may not only lead to a decrease of the S_π–S_n energy gap or even a reversed ordering of the two states in the FC region but also cause a profound modification of the topological features of the correlated potential surfaces and their interplay with the S_0 surface.[54–57,75] The latter could result in a different location and variation of the mixed character of the S_n' state as well as induce a shift in the position or variation in the barrier height associated with access to the S_n'/S_0 CI. The longer S_n' lifetime in the gas phase than in aqueous solution might reflect a relatively higher barrier from the S_n' minimum to the CI region in the former than in the latter case. In line with this, we note that time-resolved studies of thymine in less polar aprotic acetonitrile[75c] and relatively weak hydrogen-bonding ethanol[76] report τ_2 time constants of ~1–2.4 ps, following this trend and falling between the time constants observed in the aqueous solution and gas-phase studies. Taken together, this solvent tuning of the excited-state decay time shows the importance of the local environment in controlling the deactivation efficiency.

(61) (a) Lim, E. C. *J. Phys. Chem.* **1986**, *90*, 6770–6777. (b) Lai, T.-i.; Lim, E. C. *Chem. Phys. Lett.* **1980**, *73*, 244–248.

(62) Broo, A. *J. Phys. Chem. A* **1998**, *102*, 526–531.

(63) Mennucci, B.; Toniolo, A.; Tomasi, J. *J. Phys. Chem. A* **2001**, *105*, 7126–7134.

(64) Dym, S.; Hochstrasser, R. M. *J. Chem. Phys.* **1969**, *51*, 2458–2468.

(65) (a) Kearns, D. R.; Case, W. A. *J. Am. Chem. Soc.* **1966**, *88*, 5087–5097. (b) Case, W. A.; Kearns, D. R. *J. Chem. Phys.* **1970**, *52*, 2175–2191.

(66) Kang, H.; Lee, K. T.; Jung, B.; Ko, Y. J.; Kim, S. K. *J. Am. Chem. Soc.* **2002**, *124*, 12958–12959.

(67) Samoylova, E.; Lippert, H.; Ullrich, S.; Hertel, I. V.; Radloff, W.; Schultz, T. *J. Am. Chem. Soc.* **2005**, *127*, 1782–1786.

(68) Canuel, C.; Mons, M.; Piuzzi, F.; Iardivel, B.; Dimicoli, I.; Elhanine, M. *J. Chem. Phys.* **2005**, *122*, 074316.

(69) (a) He, Y.; Wu, C.; Kong, W. *J. Phys. Chem. A* **2004**, *108*, 943–949. (b) He, Y.; Wu, C.; Kong, W. *J. Phys. Chem. A* **2003**, *107*, 5145–5148.

(70) Brady, B. B.; Peteanu, L. A.; Levy, D. H. *Chem. Phys. Lett.* **1988**, *147*, 538–543.

(71) Scaiano, J. C. *J. Am. Chem. Soc.* **1980**, *102*, 7747–7753.

(72) Dalton, J. C.; Montgomery, F. C. *J. Am. Chem. Soc.* **1974**, *96*, 6230–6232.

(73) Rusakowicz, R.; Byers, G. W.; Leermakers, P. A. *J. Am. Chem. Soc.* **1971**, *93*, 3263–3266.

(74) Reichardt, C. *Solvent and Solvent Effects in Organic Chemistry*; VCH: Weinheim, Germany, 1988.

(75) (a) Santoro, F.; Barone, V.; Gustavsson, T.; Improta, R. *J. Am. Chem. Soc.* **2006**, *128*, 16312–16322. (b) Gustavsson, T.; Sarkar, N.; Lazzarotto, E.; Markovitsi, D.; Barone, V.; Improta, R. *J. Phys. Chem. B* **2006**, *110*, 12843–12847. (c) Gustavsson, T.; Sarkar, N.; Lazzarotto, E.; Markovitsi, D.; Improta, R. *Chem. Phys. Lett.* **2006**, *429*, 551–557.

(76) Häupl, T.; Wiindolph, C.; Jochum, T.; Brede, O.; Hermann, R. *Chem. Phys. Lett.* **1997**, *280*, 520–524.

The preceding observations combined with the monomer-like behavior of the $(dT)_{20}$ singlet excited states lead us to attribute the similar but clearly longer τ_2 for $(dT)_{20}$ than dT (Table 1) to the different microenvironments of these two systems. This is to be expected since the extra presence of the backbone conformation in $(dT)_{20}$ can make the thymine constituent units experience a substantially different hydration environment from what the dT monomer senses in water.[77] The less polar and more hydrophobic environment in $(dT)_{20}$ would likely lead to a longer τ_2, which is parallel to the slower τ_2 displayed by monomeric thymine in acetonitrile or ethanol compared with that in water. Furthermore, our results showing a modestly larger φ_T for $(dT)_{20}$ than dT would also likely arise from the differences in the local surroundings, analogous to a larger φ_T reported for thymine in acetonitrile relative to that in water.[10,48,78,79] However, the underlying reason for this would be associated with the change of mixed character of the S_n' state as a function of the solvent properties. It is plausible that, due to an increase of the S_π/S_n energy separation, the S_n' state becomes progressively darker and simultaneously displays a stronger SOC tendency upon decreasing the solvent hydrogen-bonding capability and polarity.[54] This may account for the larger φ_T for thymine in less polar or less hydrogen-bonding environments, such as the thymine component in $(dT)_{20}$ in water or thymine in acetonitrile, as compared with that for thymine or dT in water. Given the governing role of the T_1 state in the CPD formation, an important ramification of this environment-sensitive φ_T would be that the exact branching ratio between the prevailing and necessary photoprotective (IC) and the minor but deleterious photodamaging (ISC) channel is delicately dependent on the local properties of DNA. More experimental work and theoretical study, especially that taking into account the effect of solvent and local environmental factors, are needed to further elucidate this issue.

Conclusion

The present study demonstrates how the molecular evolution of the photoexcited dT monomer and $(dT)_{20}$ oligomer can be characterized directly and monitored in real time on the femtosecond to early picosecond time scales using time-resolved broadband spectroscopy. Our results show explicitly that, for both systems, there is a rapid branching of the excited-state population between two decay channels with the predominant pathway leading to excitation elimination and recovery of the S_0 state and a minor pathway resulting in ISC conversion to the photoreactive T_1 state. Temporal evolution of our combined and complementary TA and TRF spectra provides solid evidence for the involvement of a doorway state of singlet nature to facilitate bifurcation of the initial S_π population to either the S_0 or T_1 states. The spectral features and related conversion dynamics observed for this state indicate that it is associated with a S_n' state of mixed nature and that this state likely results from vibrational coupling of the S_π state to an energetically nearby S_n state. A common but distinct stepwise deactivation mechanism is proposed for the two compounds to account for their photostability in aqueous environment. Comparison of the spectral evolution and the decay dynamics for dT and $(dT)_{20}$ reveals a single base localized character for not only the initial

photoexcitation but also the ensuing relaxation processes in the thymine oligomer. The observation of much faster T_1 decay dynamics in $(dT)_{20}$ than dT enables an "intrinsic" triplet pathway to be revealed for the DNA CPD formation. Our study also shows that, although the modification of the local environment introduced by the oligomer assembly does not qualitatively alter the overall excited-state relaxation pathway and reaction channels of the T_1 state, the intrastrand T_1 self-quenching reaction is greatly facilitated in $(dT)_{20}$ (featured by ~140 ps time constant) due to the close spatial proximity of adjacent thymine components and the highly flexible character of the thymine oligomer chain. This renders the T_1 state to be a very efficient precursor to yield CPD in a thymine oligomer. This may represent a general path to account for most of the CPD photodamage observed generally in various DNA systems. To further confirm this and to explore how base sequences and conformation properties may affect the DNA propensity for CPD damage, we plan to extend our time-resolved studies to other related single-stranded and double-stranded oligomer systems. We hope that the spectral and dynamical data presented here can help to supply essential experimental information to encourage corresponding theoretical investigations that can supply more insight so as to achieve a comprehensive consensus on the molecular origin of photostability and photodamage for both monomeric and oligomeric thymine systems in aqueous solution.

Supporting Information Available: Detailed comparison of the UV-absorption and initial TRF spectra for dT and $(dT)_{20}$, dynamics of the S_0 vibrational cooling resulting from the ultrafast IC decay of the photoexcited state, detailed spectral parameters obtained for the initial and late time spectra of dT and $(dT)_{20}$, extraction of the intrinsic spectra of the S_π and S_n' states based on TRF spectral analysis, estimation of the fluorescence quantum yield for dT and $(dT)_{20}$ based on the Strickler–Berg equation for a correlation of the steady-state UV absorption and the measured TRF spectra, Figure 1S showing full scale TA spectra obtained for dT and $(dT)_{20}$ with 267 nm excitation in buffered aqueous solution, Figure 2S showing representative $(dT)_{20}$ TA spectra recorded at late picosecond times with 267 nm excitation in aqueous solution, Figure 3S showing experimental and log-normal fitted TRF spectra for dT and $(dT)_{20}$, Figure 4S showing intrinsic fluorescence spectra determined for the S_π and S_n' states of dT and $(dT)_{20}$ based on dynamical analysis of the corresponding TRF spectra, Figure 5S showing UV absorption of dT and $(dT)_{20}$ recorded before and after the time-resolved experiments and Table 1S providing spectral parameters obtained from the log-normal simulations of the dT and $(dT)_{20}$ TRF fluorescence spectra. This material is available free of charge via the Internet at http://pubs.acs.org.

JA077831Q

(77) (a) Shishkin, O. V.; Gorb, L.; Leszczynski, J. *Int. J. Mol. Sci.* **2000**, *1*, 17–27. (b) Shishkin, O. V.; Hobza, P.; Leszczynski, J. *Int. J. Quantum Chem.* **2000**, *80*, 1116–1124.
(78) Salet, C.; Bensasson, R. *Photochem. Photobiol.* **1975**, *22*, 231–235.
(79) Becker, R.; Kogan, G. *Photochem. Photobiol.* **1980**, *31*, 5–13.